Journal of Fluorescence (2019) 29:673–682
https://doi.org/10.1007/s10895-019-02375-3

ORIGINAL ARTICLE

Intense Yellow Emitting Biocompatible CaS:Eu Nanophosphors Synthesized by Wet Chemical Method

S. Rekha [1,2] · E. I. Anila [2]

Received: 22 January 2019 / Accepted: 28 March 2019 / Published online: 29 April 2019

Abstract

Here we report the synthesis of intense yellow emitting CaS:Eu nanoparticles by a low temperature wet chemical coprecipitation method which can be used for various optoelectronic and biological applications. The particles were characterized systematically using techniques such as X-ray diffraction (XRD), field emission scanning electron microscopy, transmission electron microscopy (TEM), X-ray photoelectron spectroscopy, photoluminescence (PL) and UV-Vis absorption spectroscopy. XRD analysis revealed that all the samples exhibited a cubic structure with good crystallinity. Formation of nanoparticles having spherical morphology with the diameter in the range 4–8 nm was confirmed by TEM analysis. The PL emission color varied from yellowish white to yellow as the excitation wavelength was increased from 335 to 395 nm. The PL emission peaks are attributed to $^5D_0$- ^7F_J (J = 0,1,2,3,...) electronic transitions of Eu^{3+} ions incorporated into the CaS host lattice. Fourier transform infrared spectroscopy measurements were taken to elucidate the presence of various bonds in the sample. In vitro cytotoxicity analysis of the samples was also performed using MTT assay on human L929 fibroblasts cell lines in order to assess the biocompatibility of the nanoparticles. This is the first time report of the cytotoxicity studies of highly fluorescent CaS: Eu nanoparticles synthesized by wet chemical method.

Keywords Nanophosphors · Chemical coprecipitation · Photoluminescence · Cytotoxicity

Introduction

Sulfide-based luminescent materials have attracted considerable attention because of their wide range of photoluminescence and electroluminescence applications. The luminescence of alkaline earth metal sulfides like MgS, SrS, CaS and BaS doped with various activators has been studied extensively by many researchers. Of these alkaline earth sulfides, CaS is an excellent luminescent material having a wide bandgap (4.5 eV) and size-tunable optical properties [1–4]. On doping with various dopants like rare earth ions, the luminescence of CaS can be varied over the entire visible region. Rare earth ions are also known as lanthanides, and they are most stable in triply ionized form. The emission of lanthanide ions is due to their intra 4f electronic transitions which yield only a weak fluorescence. When they are incorporated into a host matrix, the luminescence can be improved by the intermixing of the 4f states with the ligands of the host matrix and excitation to d electronic states due to crystal field effects. Recently trivalent lanthanide ions doped semiconductor nanophosphors have gained significant importance because of their applications in diverse fields such as optoelectronics, lighting technology, flat panel displays and luminescent biolabels [5–7]. Of the many rare earth ions, europium is an important dopant element giving emission from UV to red region of the electromagnetic spectrum.

Different methods have been employed for the synthesis of europium doped CaS nanoparticles by researchers. Sun et al. [8] synthesized Eu^{2+} doped CaS nanoparticles for the first time by a wet chemical method. The prepared nanoparticles had a very low fluorescence intensity before annealing at high temperatures because of their poor crystallinity. Sawada et al. [9] prepared Eu^{2+} doped CaS nanoparticles by alkoxide method which exhibited photoluminescence emission on heating at 700 °C in the presence of N_2. The luminescence properties of micrometer-sized europium doped CaS synthesized using

✉ E. I. Anila
anilaei@gmail.com

[1] Department of Physics, Maharaja's College, Ernakulam, Kerala, India

[2] Optoelectronic and Nanomaterials Research Laboratory, Department of Physics, Union Christian College, Aluva, Kerala 683102, India

solvothermal method was studied by Haecke et al. [10]. Burbano et al. [11, 12] studied the near IR photoluminescence of CaS: Eu^{2+} nanoparticles synthesized using wet chemical coprecipitation method which has potential applications in optical information storage. In all the reports mentioned above the valence state of europium in CaS host lattice was found to be Eu^{2+}, and the PL emission spectra consisted of an intense peak in the red region due to $4f^6\ 5d^1 \rightarrow 4f^7$ transition of Eu^{2+}. Only a few reports are available on the synthesis of nanosized Eu^{3+} doped CaS phosphors having good crystallinity and high fluorescence intensity [13, 14]. Wet chemical method is a simple and low-cost method for the synthesis of nanoparticles with some desirable prerequisites, such as controlled composition and crystal phase, tailored geometric parameters and ease of processability. In this paper, we report color tunable emissions of Eu^{3+} doped CaS nanophosphors synthesized by a wet chemical method using triethanolamine (TEOA) as a capping agent and their structural and optical characterization using various techniques. The CIE chromaticity coordinates of all the samples have been evaluated, and the chromaticity diagram is also plotted. X-ray photoelectron spectroscopy (XPS) was used to determine the valence state of Eu in CaS. Literature reports reveal that CaS nanoparticles are promising candidates for various biomedical applications including diagnosis and treatment of cancer [15–17]. For the safe use of these nanoparticles in biomedicine a detailed understanding of the biocompatibility and toxicity of these particles in human beings is necessary. With this aim we have conducted the in vitro cytotoxicity studies of TEOA capped CaS:Eu nanophosphors on human L929 fibroblasts cells using MTT assay.

Experimental

Synthesis of CaS:Eu Nanophosphors

Europium-doped CaS nanophosphors capped with TEOA were synthesized using a wet chemical coprecipitation method [8, 18]. The starting materials used were calcium chloride [$CaCl_2.\ 2H_2O$, 97% Merck], sodium sulfide [$Na_2S.xH_2O$,Merck] and europium acetate [$Eu(OOCCH_3)_3$, Alpha aesar 99.9%]. Initially $CaCl_2.2H_2O$ (0.5 M) and $Na_2S.xH_2O$ (0.5 M) were dissolved separately in 50 mL of 2-propanol. To 50 mL solution of Na_2S, the capping agent TEOA (1 mL) was added. Here TEOA is used for surface modification of the nanoparticles which increases its stability and intensity of photoluminescence. The required molar concentration (0.03 M, 0.04 M, 0.05 M, 0.06 M, and 0.07 M) of Europium acetate was also prepared in 2-propanol and added to calcium chloride solution. Then sodium sulfide solution was added dropwise to the mixture of $CaCl_2$ and $Eu(OOCCH_3)_3$ under continuous stirring. The solution was vigorously stirred for 2 h followed by heating at 80 °C so that its volume reduces to one-fourth the original volume. To this solution, 20 mL of tetrahydrofuran was added and stirred for about 30 min. It was then filtered, washed with 2-propanol and dried in a hot air oven at 80 °C for 6–8 h to obtain the nanoparticles. Uncapped CaS: Eu nanoparticles were also prepared using the same method without adding the capping agent TEOA.

In Vitro Toxicological Analysis Using MTT Assay

MTT assay is the most widely used assay, and it stands for 3 (−4,5-Dimethylthiazol-2-yl)2,5- diphenyltetrazolium bromide. The mitochondrial dehydrogenase of living cells cleaves the tetrazolium ring of the colorless MTT and convert it into purple MTT formazan crystals which do not dissolve in aqueous solution. Formazan crystals are then dissolved using a solubilizing solution and absorbance is measured. If the production of MTT formazan is more, greater will be the number of viable cells [19].

L929 (Fibroblast) cells were procured from National Centre for Cell Sciences (NCCS), Pune, India and maintained in Dulbecco's modified Eagles medium, DMEM (Sigma Aldrich, USA). The cell line was cultured in 25 cm^2 tissue culture flask with DMEM supplemented with 10% fetal bovine serum(FBS), L-glutamine, sodium bicarbonate (Merck, Germany) and antibiotic solution. The cultured cells were seeded in 96 well tissue culture plate at a density of 5×10^4 cells /well and incubated at 37 °C in a humidified 5% CO_2 incubator. After 24 h the growth medium was removed, and the cells were incubated with different concentrations of CaS: Eu nanoparticles (6.25-100 μg/ml)). Non-treated control cells were also maintained for analysis. The sample contents were removed after 24 h of incubation, and MTT (Sigma Aldrich, M-5655) assay test was performed on both the test and control cells following a standard protocol. The absorbance values were recorded by using a microplate reader at a wavelength of 540 nm [20]. Qualitative visual characterization was also performed by taking phase-contrast microscopic images of the control and cells treated with different concentrations of CaS:Eu nanoparticles in order to assess the cell viability.

Measurements

Crystalline nature and phase formation of CaS nanoparticles were examined using X-ray diffraction (XRD) patterns which were recorded by Bruker AXS D8 Advance instrument by employing Cu-Kα lines (λ = 1.5406 Å). The morphology of the particles was studied using a Carl Zeiss Field Emission Scanning Electron Microscope (FESEM) and a Jeol/Jem 2100 model Transmission Electron Microscope (TEM). The Photoluminescence emission (PL) spectra of the samples were registered with Flouromax4C spectrofluorometer having a

150 W ozone free Xenon lamp as an excitation source. The Diffuse Reflectance Spectra (DRS) was recorded using a UV-Vis-NIR spectrophotometer (Varian, Cary5000). A Thermo Scientific K-Alpha model instrument having an AI K-alpha X-ray source (1486.68 eV) was employed for conducting XPS analysis. The Fourier Transform Infrared (FTIR) spectrum of the prepared nanoparticles was recorded using a Thermo Nicolet, Avatar 370, FTIR spectrometer. For cytotoxicity studies, absorbance values of the control and cells treated with samples were measured using an Erba, Germany microplate reader and the microscopic observations were recorded using a phase contrast microscope (Olympus CKX41 with Optika Pro5 CCD camera).

Results and Discussion

TEM /FESEM Analysis

The morphology and particle size of the nanophosphors were examined using TEM and FESEM analysis. The TEM micrographs of TEOA capped CaS:Eu nanophosphors is shown in Fig. 1a, and it confirms the formation of nanoparticles having a nearly spherical morphology. HRTEM is a useful technique to determine the particle size and gives authentic information about particle size distribution and structure of the particles. The HRTEM image of CaS:Eu nanoparticles capped with TEOA is depicted in Fig. 1b from which it is evident that the diameter of the particles is less than 10 nm. The structure of the CaS: Eu nanoparticles was revealed by the selected area diffraction (SAED) pattern depicted in Fig. 1c which consists of three concentric rings corresponding to the diffraction planes (111), (200) and (220) of CaS cubic phase. Hence the crystallinity and cubic phase of the nanoparticles formed are confirmed by the SAED pattern. The size distribution of CaS: Eu nanoparticles (Fig. 2a) is obtained from TEM analysis which reveals that most of the particles have a diameter in the range 5–6 nm. Figure 2b gives the FESEM image of TEOA capped CaS:Eu nanoparticles which also shows that the particles have a spherical morphology. FESEM image shows large particles that are aggregates of a large number of small nanoparticles. Hence TEM/FESEM analysis give evidence for the crystalline nature, cubic phase and nanoscale size of the synthesized particles.

XRD Analysis

The XRD pattern of europium doped CaS nanophosphors is depicted in Fig. 3 which is in good agreement with the standard data available in JCPDS card No:77–2011. The XRD pattern consists of major diffraction peaks at (111), (200), (220), (222), (400) and (420) corresponding to the cubic crystalline phase of CaS. Two weak peaks at 2θ values around 36^0 and 39^0 are observed in the XRD spectrum of uncapped CaS: Eu which are due to the presence of additional phase of calcium oxide and calcium hydroxide in the samples. However, TEOA capped CaS:Eu does not contain any impurity peaks corresponding to the secondary phase which shows that they have better purity. To calculate the average crystallite size of the nanoparticles formed we used the Scherrer formula [21] which is expressed as:

$$D = \frac{0.9\lambda}{\beta\cos\theta} \tag{1}$$

where D is the average crystallite size of the particles, λ is the wavelength of the Cu-Kα (1.5406 Å) radiation, β (in radian) is the full width at half maximum (FWHM), and θ is the diffraction angle of an observed peak. The lattice parameter was calculated using the equation,

$$d_{hkl} = \frac{a}{\sqrt{h^2 + k^2 + l^2}} \tag{2}$$

where d_{hkl} represents the interplanar distance, a represents the lattice parameter and h, k, l represents the Miller indices. The calculated values of average crystallite size and lattice parameter of uncapped and capped europium doped CaS

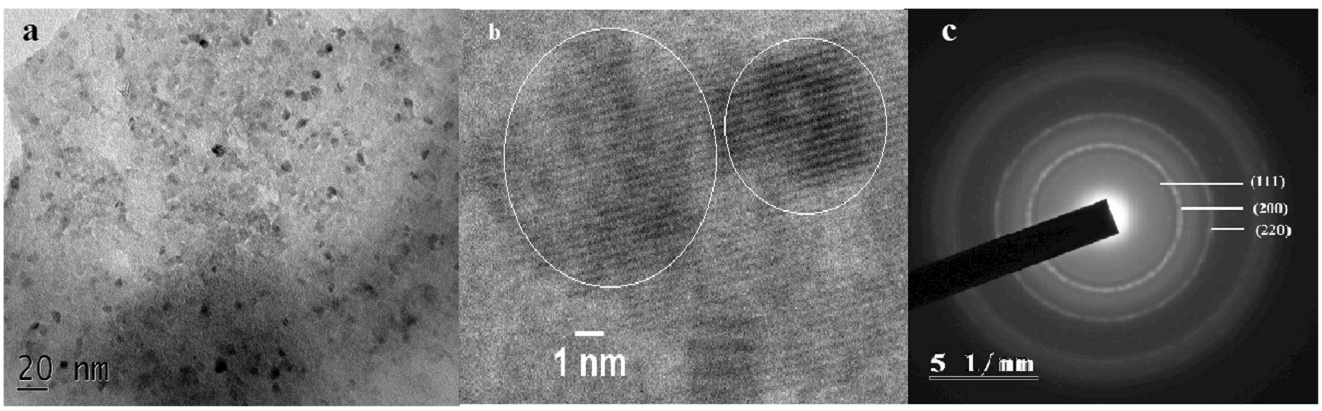

Fig. 1 **a** TEM, **b** HRTEM and **c** SAED pattern of TEOA capped CaS:Eu nanoparticles

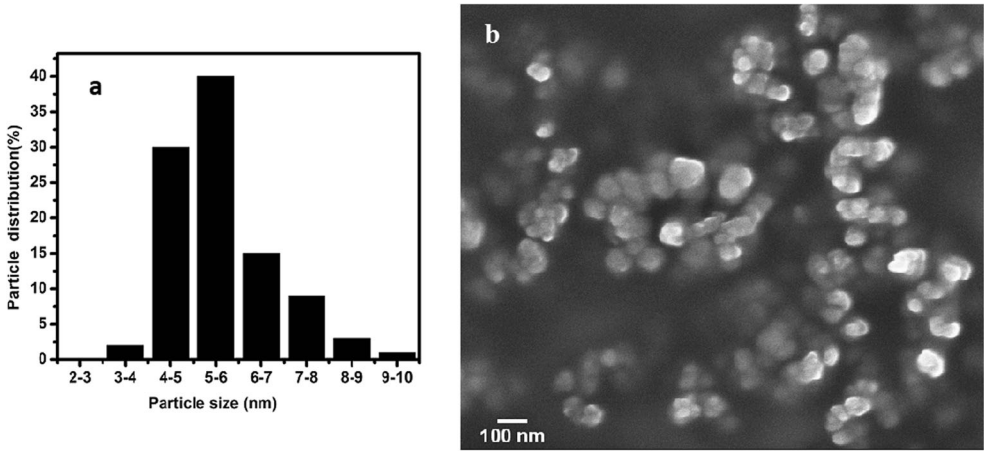

Fig. 2 **a** Particle distribution histogram and **b** FESEM image of TEOA capped CaS:Eu nanoparticles

nanophosphors are tabulated in Table 1. Although there is no considerable reduction in particle size due to capping we observed the stability of the nanoparticles had been increased due to the addition of TEOA. The value of the ionic radius of Eu^{3+} ion (0.95 Å) is lesser than the ionic radius of Ca^{2+} ion (1.14 Å), and hence a decrease in lattice parameter from the bulk value is observed on doping due to this lattice mismatch. The peak positions of the diffraction peaks shift towards high angle region due to this decrease in the value of the lattice parameter. Hence the synthesized phosphors possess phase purity, stability, and high crystallinity which are desirable for exhibiting better photoluminescent properties.

PL Studies

The PL emission spectrum of europium is strongly related to the host lattice and can occur from UV to visible region of the electromagnetic spectrum. This is because the 5d → 4f transitions of europium are linked with changes in electric dipole and 5d excited state is influenced by crystal field effects. The PL emission spectra of undoped and europium doped CaS nanoparticles were recorded at room temperature for excitation wavelengths 335 nm and 365 nm. Figure 4a gives emission spectra of various samples for an excitation wavelength of 335 nm. From the figure, it is evident that for pure CaS sample capped with TEOA, the emission spectrum consists of a broad peak in the range 375–500 nm attributed to intrinsic point defects present in the host lattice whereas for all capped CaS: Eu samples the emission spectra consist of peaks at 590 nm and 613 nm corresponding to ($^5D_0 \rightarrow {}^7F_1$) and ($^5D_0 \rightarrow {}^7F_2$) electronic transitions of europium [22, 23]. From the figure, it is found that for uncapped CaS doped with 0.03 M Eu, the emission spectrum consists of a broad peak around 600 nm corresponding to 5d → 4f transitions of europium. Also, the PL intensity of this sample is found to be lower than that of capped CaS: Eu nanophosphors having the same concentration of europium (0.03 M) which shows that capping has resulted in the enhancement of PL intensity. The intensity of the peaks at 590 nm and 613 nm increases with dopant concentration. Enhancement of Eu emission shows that CaS nanocrystals have absorbed energy from the excitation source and transferred this energy by non-radiative recombination to Eu ions which act as luminescence centers. The PL emission intensity reaches a maximum value for 0.06 M of Eu concentration and further decreases with increase in the concentration of europium due to concentration quenching.

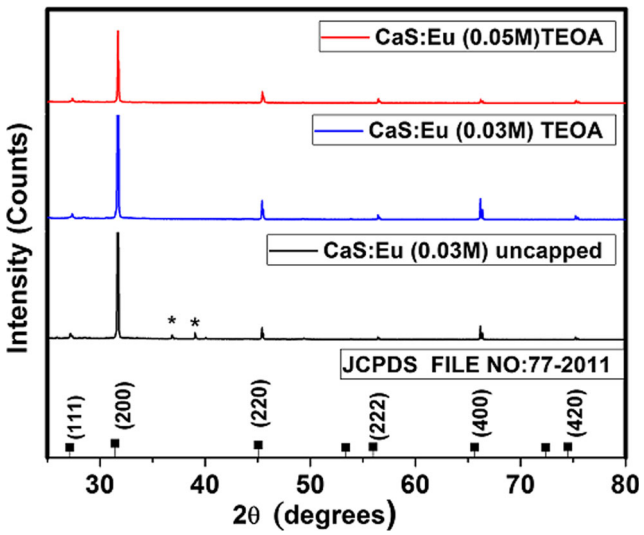

Fig. 3 XRD pattern of Eu doped CaS nanophosphors

The PL emission spectra of europium doped CaS nanoparticles for an excitation wavelength 395 nm is displayed in Fig. 4b which consists of sharp peaks at 590 nm and 613 nm and minor peaks at 538 nm, 578 nm, 649 nm, 699 nm and 754 nm due to electronic transitions from the excited state ^5D_i (where i = 0,1) to ^7F_J (where J = 0,1,2,3.....). From the figure, it is also evident that pure CaS do not give any emission for this excitation wavelength. The PL intensity of TEOA capped CaS nanophosphor is greater than that of uncapped CaS having the same concentration of Eu (0.03 M). The emission peak

Table 1 Average crystallite size and lattice parameter of CaS:Eu nanophosphors

Sample name	Average crystallite size from Scherrer formula (nm)	Lattice parameter(Å)
CaS bulk	_	5.689
CaS:Eu(0.03 M) uncapped	30	5.641
CaS:Eu (0.03 M) TEOA	28	5.640
CaS:Eu (0.05 M) TEOA	28	5.635

at 590 nm ($^5D_0 \rightarrow {}^7F_1$) is due to the magnetic dipole transition, and this transition reflects the site symmetry of the Eu^{3+} ion [22–26]. The intensity of this magnetic dipole allowed transition is independent of the local environment. The peak at 613 nm ($^5D_0 \rightarrow {}^7F_2$) is allowed by electric dipole moment, and it is called hypersensitive transition since it is very sensitive to the local environment of Eu^{3+} ion and depends on the symmetry of the crystal field. The other weak emissions at 538 nm, 578 nm, 649 nm, 699 nm and 754 nm are due to the($^5D_1 \rightarrow {}^7F_1$), ($^5D_0 \rightarrow {}^7F_0$)), ($^5D_0 \rightarrow {}^7F_3$) ($^5D_0 \rightarrow {}^7F_4$) an($^5D_0 \rightarrow {}^7F_5$) transitions respectively [23, 25, 26].

It is observed that in the case of TEOA capped CaS:Eu nanophosphors, as the concentration of europium, is increased the intensity of $^5D_0 \rightarrow {}^7F_J$ transitions also increase. The PL intensity reaches the maximum value for 0.06 M Eu^{3+} concentration, and beyond this, it declines due to the phenomenon of concentration quenching which occurs as a consequence of non-radiative energy transfer between neighboring Eu^{3+} ions. This non-radiative energy transfer occurs due to exchange interaction, radiative reabsorption or by multipole-multipole interactions. The PL intensity generally increases as the effective distance between Eu^{3+} ion decreases. However, when the concentration increases beyond the critical value, as the distance between the Eu^{3+}ions decreases non-radiative relaxation occurs resulting in a decrease of PL intensity. This energy transfer depends on the critical distance R_C between Eu^{3+}ions which can be calculated using the equation given by Blasse which is as follows,

$$R_C \approx 2\left(\frac{3V}{4\pi \mathrm{Xc\ N}}\right)^{1/3} \tag{3}$$

where X_c is the critical concentration of the dopant, N is the number of Ca^{2+} ion in the unit cell, and V is the volume of the unit cell [27, 28]. For CaS, $X_c = 0.06$, $N = 4$ and volume V = 0.1789 nm^3. Using these values, the critical distance R_C is obtained as 11 Å. Since the value of R_C is greater than 5 Å, the exchange interaction is no more effective. Hence it can be concluded that concentration quenching is attributed to multipole -multipole interaction between Eu^{3+} ions.

The intensity ratio of ($^5D_0 \rightarrow {}^7F_2$) to ($^5D_0 \rightarrow {}^7F_1$) transition is called asymmetry ratio and is related to the local environment of Eu^{3+} ions. Larger the intensity ratio, lower will be the local symmetry denoting the absence of a center of symmetry in the host lattice [23, 25, 26]. In a weak crystal field, the Eu^{3+} ion has high octahedral stabilization energy, and the Eu^{3+} ions will occupy octahedral sites of Ca^{2+}. The asymmetry ratio for various samples for excitation wavelength 395 nm is calculated and tabulated in Table 2. From these values, we can conclude that Eu^{3+} ions occupy the non-centrosymmetric octahedral sites in the surface of CaS nanocrystals. From the table, it is evident that the asymmetry ratio increases with the

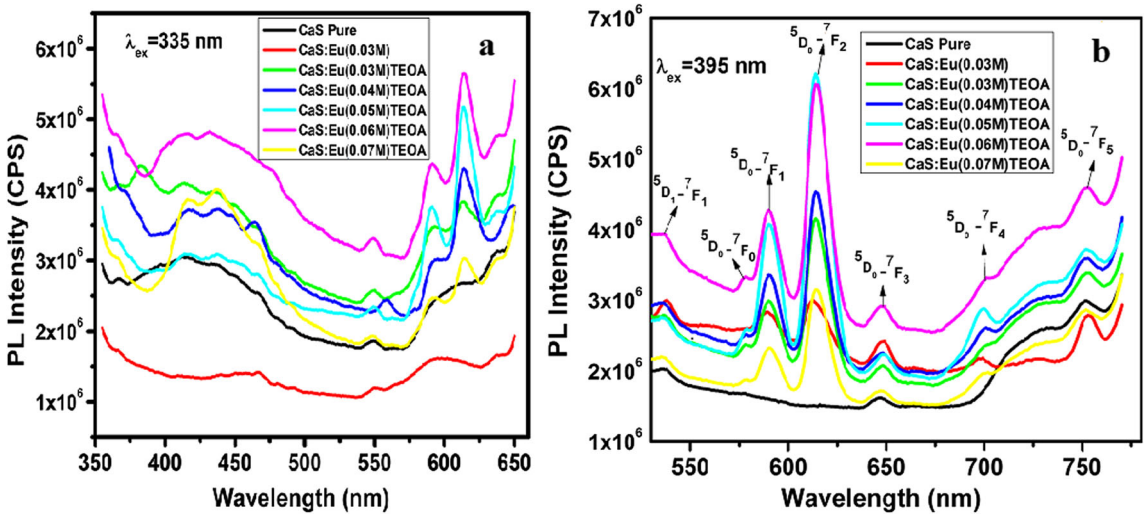

Fig. 4 PL spectra of CaS:Eu nanoparticles for an excitation wavelength **a** 335 nm and **b** 395 nm

Table 2 Asymmetry ratio and the bandgap of CaS:Eu nanophosphors

Sample	Asymmetry ratio	Bandgap E_g (eV)
CaS:Eu (0.03 M) uncapped	1.65	4.27
CaS:Eu (0.03 M) TEOA	2.31	4.48
CaS:Eu (0.04 M) TEOA	2.97	4.30
CaS:Eu (0.05 M) TEOA	2.99	4.33
CaS:Eu (0.06 M) TEOA	2.81	4.19
CaS:Eu(0.07 M) TEOA	2.68	4.01

concentration of europium and its maximum value is for 0.05 M of europium doped samples. Its value decreases with further increase in doping concentration.

The Commission Internationale de l'Eclairage (CIE) coordinates (x,y) of CaS:Eu phosphors are calculated from the PL emission spectra data in order to analyze the performance and color purity of the synthesized phosphor. The color of any object can be conveniently represented by a point on the CIE chromaticity diagram through its color coordinates. The CIE color coordinates of Eu doped CaS nanophosphors for excitation wavelengths 335 nm and 395 nm are calculated and tabulated in Table 3. The chromaticity diagram was plotted (Fig. 5), and it was found that for an excitation wavelength 335 nm the chromaticity coordinates of all samples fall in the yellowish white region (close to the standard white light point). This may occur due to the existence of defect-related emissions along with orange and red emissions. For 395 nm excitation, the chromaticity coordinates of all samples fall in the yellow region as shown in Fig. 5. Here even though the red emission is stronger the resultant emission color is yellow due to the overlapping of red, orange and defect-related blue emissions.

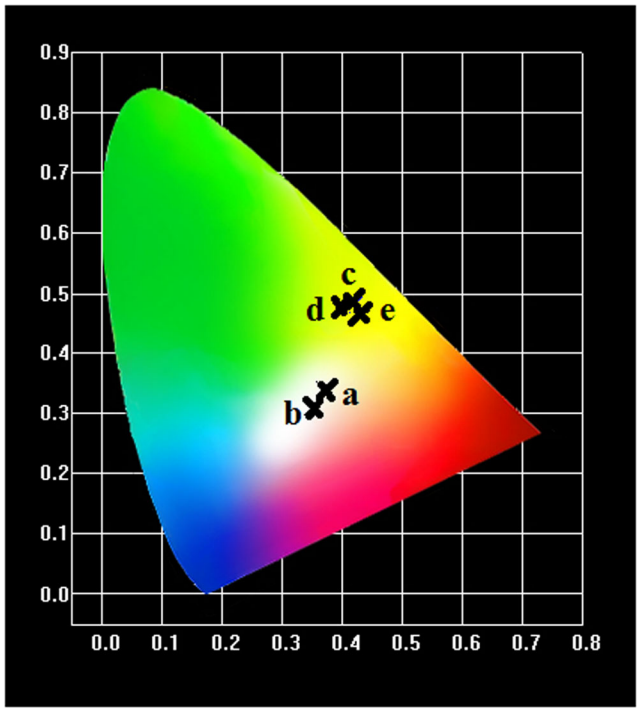

Fig. 5 CIE chromaticity diagram of CaS:Eu nanophosphors. Point a corresponds to 0.03 M uncapped &0.04 M Eu doped samples, point b corresponds to 0.03 M, 0.05 M, 0.06 M & 0.07 M Eu doped CaS nanophosphors for an excitation wavelength 335 nm. Point c corresponds to 0.03 M undoped; point d corresponds to 0.03 M, 0.04 M, 0.06 M & 0.07 M Eu doped samples and point e corresponds to 0.05 M Eu doped CaS nanophosphors for excitation wavelength 395 nm

DRS Analysis

The DRS of the CaS:Eu nanoparticles are depicted in Fig. 6(1) which shows increased reflectance in the visible region for all the samples. The optical band gap of the nanoparticles can be

Table 3 CIE coordinates of CaS:Eu nanophosphors for excitation wavelengths 335 and 395 nm

Excitation wavelength (nm)	Sample	CIE coordinates	
		x	y
335	CaS:Eu (0.03 M)uncapped	0.37	0.34
	CaS:Eu (0.03 M)TEOA	0.35	0.31
	CaS:Eu (0.04 M)TEOA	0.37	0.34
	CaS:Eu (0.05 M)TEOA	0.34	0.31
	CaS:Eu (0.06 M)TEOA	0.34	0.31
	CaS:Eu (0.07 M)TEOA	0.34	0.30
395	CaS:Eu (0.03 M)uncapped	0.42	0.48
	CaS:Eu (0.03 M)TEOA	0.40	0.48
	CaS:Eu (0.04 M)TEOA	0.40	0.48
	CaS:Eu (0.05 M)TEOA	0.43	0.47
	CaS:Eu (0.06 M)TEOA	0.40	0.48
	CaS:Eu (0.07 M)TEOA	0.40	0.48

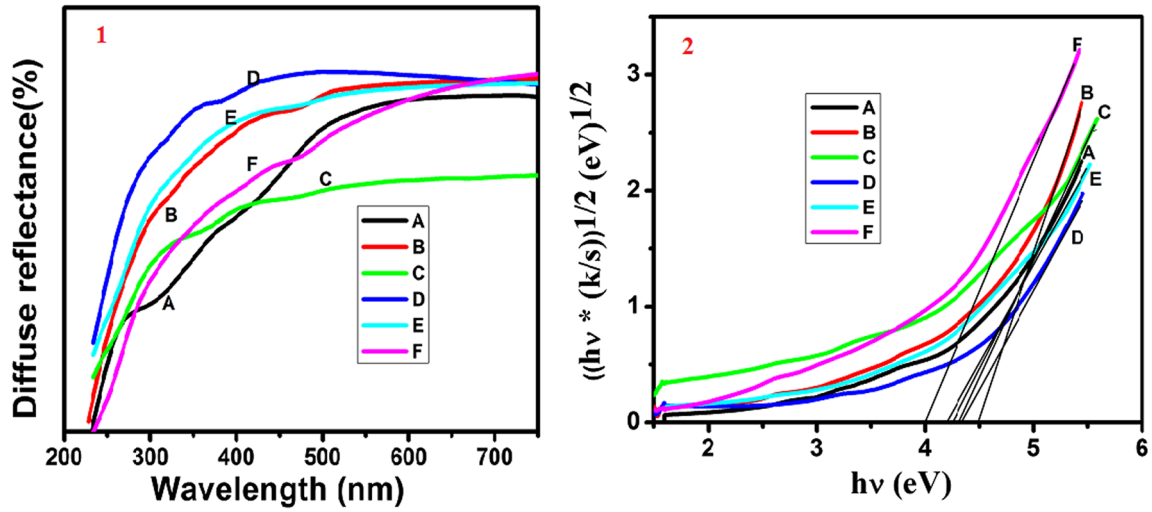

Fig. 6 **1** DRS and **2** (hν * (k/s))$^{1/2}$ versus hν curves of A) CaS:Eu (0.03 M)uncapped, B) CaS:Eu (0.03 M) TEOA, C) CaS:Eu (0.04 M) TEOA, D) CaS:Eu (0.05 M) TEOA, E) CaS:Eu (0.06 M) TEOA and F) CaS:Eu (0.07 M) TEOA capped nanophosphors

determined from the Kubelka-Munk relation given by,

$$F(R) = \frac{(1-R)^2}{2R} = \frac{k}{s} \quad (4)$$

where F(R) is the Kubelka-Munk function, R is the diffuse reflectance, k is the absorption coefficient, and s is the scattering coefficient [29, 30]. The value of [k/s * hν]$^{1/2}$ is calculated from the DRS data, and a graph is plotted with energy hν along X-axis and [k/s * hν]$^{1/2}$ along Y-axis [Fig. 6(2)] to obtain the bandgap E_g of the samples which is displayed in Table 2. The value of band gap for TEOA capped CaS:Eu (0.03 M) is found to be greater than that of uncapped CaS: Eu (0.03 M) which may be attributed to the decrease in particle size on capping. The bandgap of all TEOA capped CaS:Eu nanophosphors are found to be lower than that obtained for undoped TEOA capped CaS nanophosphor in our previous work [31] which may be attributed to band tailing effect [32, 33] caused by the narrowing of bandgap due to increase in carriers and interaction between the carriers and impurities present in the samples. The decreasing trend in bandgap for capped samples with increase in doping concentration can also be attributed to the same effect.

XPS Analysis

XPS analysis of TEOA capped CaS:Eu nanoparticles was carried out to identify the presence of the elements calcium, sulfur and europium and their valence states in the host CaS matrix. Figure 7a–c depicts the high-resolution XPS spectra of Ca 2p, S 2p, and Eu 3d. The peaks at 347.2 and 350.6 eV are associated with Ca $^2p_{3/2}$ and Ca $^2p_{1/2}$, and the difference in binding energy is 3.4 eV which indicates the divalent state of Ca ion in the CaS crystal lattice [34]. The peak at 167 eV is associated with S 2p level [13, 34]. The core level binding energies of Eu $^3d_{3/2}$ and Eu $^3d_{5/2}$ are found to be 1164.8 and1135.3 eV respectively which shows that Eu ions are present in a trivalent state on the surface of the host lattice [13, 34–36]. Thus from XPS analysis, it is evident that Eu^{3+} ions are successfully incorporated into the CaS lattice.

Cytotoxicity Analysis

For cytotoxicity studies, 0.06 M Eu doped CaS nanoparticles were used since they exhibit optimum PL intensity. L929 fibroblasts cells were treated with varying concentrations of

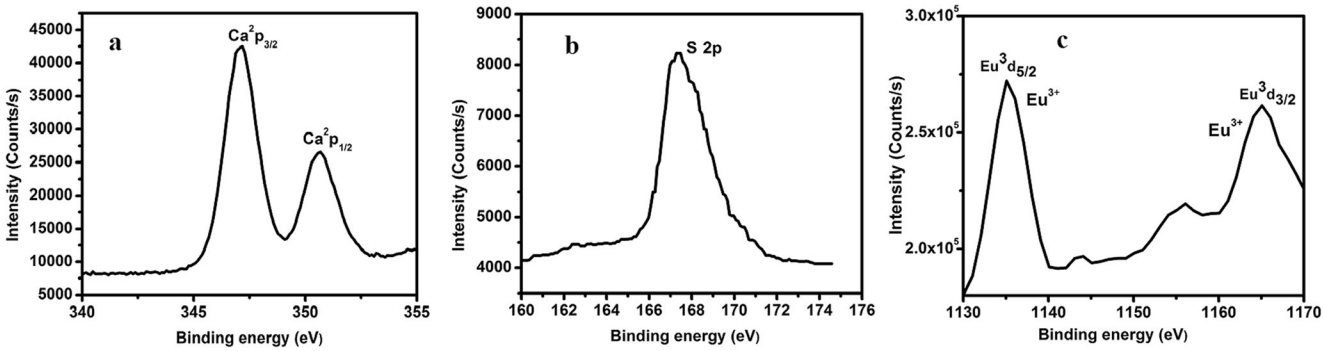

Fig. 7 XPS of **a** Ca2p **b** S2p and **c** Eu3d core levels for TEOA capped CaS:Eu (0.03 M) nanophosphors

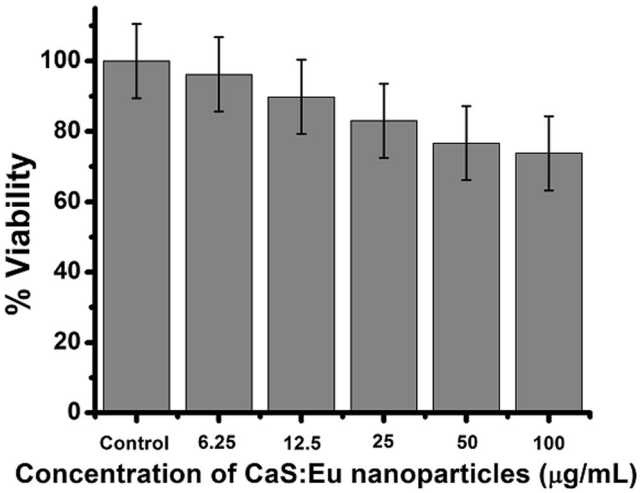

Fig. 8 Graph showing percentage viability versus concentration of CaS:Eu nanoparticles using MTT assay after 24 h of incubation

CaS: Eu nanophosphors and cell viability were estimated from MTT assay method. The percentage of viability was determined using the formula:

$$\text{Percentage of viability} = \frac{\text{Mean OD of the Samples}}{\text{Mean OD of the control group}} \times 100 \quad (5)$$

where OD represents the optical density of the samples. Cell viability of all the test groups (6.25 to 100 μg/mL) was calculated to be more than 70%. Figure 8 illustrates the cytotoxicity analysis results using MTT assay which was conducted to check the cell survival rate after 24 h of incubation with CaS: Eu nanoparticles. Mean of the average OD of the samples were different from the control group, but the viability of the cells were more than 70% in all the samples tested which is well above the 70% cut off for cytotoxicity as recommended by ISO 10993-5: 2009 (Biological evaluation of medical devices part-5: Tests for in-vitro cytotoxicity). Hence our results show that the cells remain viable for all the dosages treated with relatively higher viability (90–80%) for lower dosages of the sample. From Fig. 8 it is evident that as the concentration of the sample increases the number of viable cells also decreases. The concentration of the sample which inhibits 50% of the cells is denoted by IC_{50}, and its value is found to be 197 μg/mL (Calculated using ED50 PLUS V1.0 Software).

The entire plate was observed after 24 h of treatment of the samples in an inverted phase contrast tissue culture microscope, and microscopic observation was recorded as images. Figure 9a–f gives the microscopic images of the control group

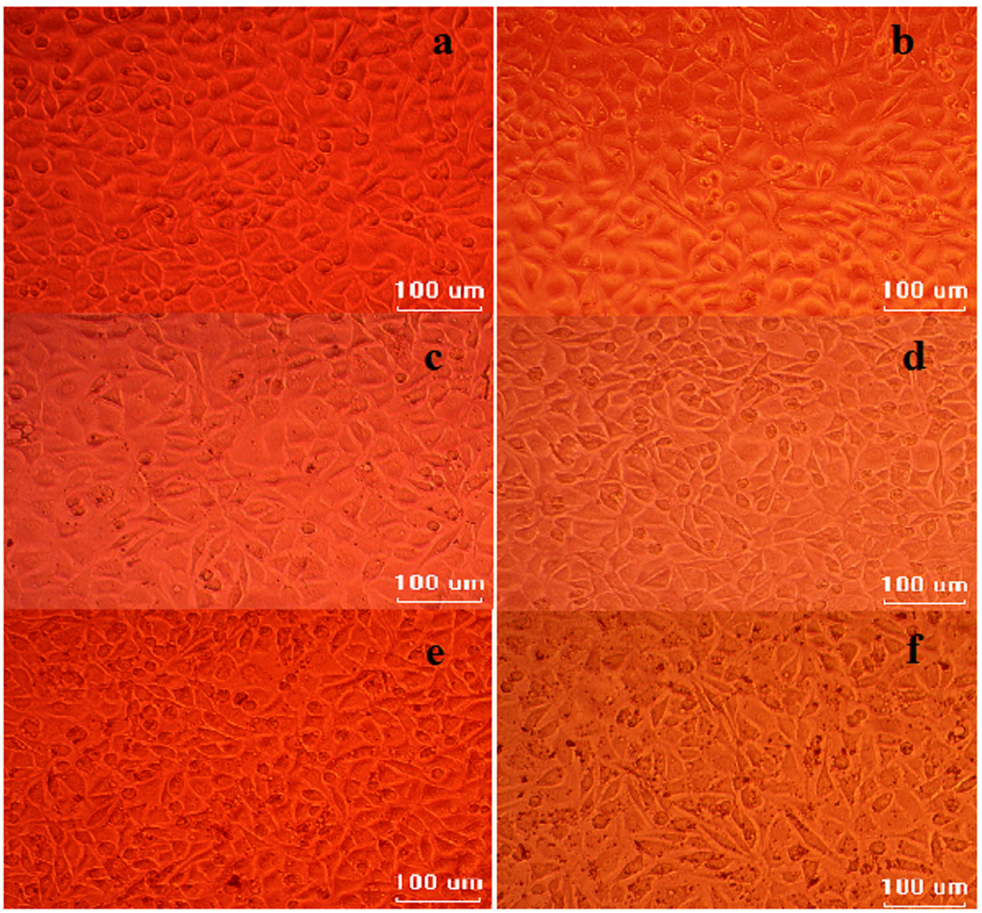

Fig. 9 Microscopic images of L929 human fibroblasts cells treated with varying concentration of CaS:Eu nanoparticles **a** control **b** 6.25 **c** 12.5 **d** 25 **e** 50 and **f** 100 (μg/mL) of CaS:Eu nanoparticles

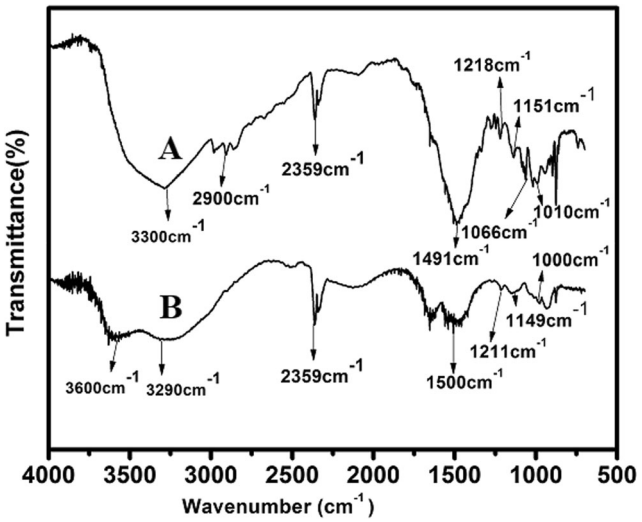

Fig. 10 FTIR spectra of **a** TEOA capped CaS:Eu (0.03 M) and **b** uncapped CaS:Eu (0.03 M) nanophosphors

and the test groups treated with varying concentration of the sample. From the images, we can see that the addition of nanoparticles up to 50 μg/ ml have not brought considerable changes in the cells and all the images are almost identical to that of the control. Also, there is no visible change in morphology of the cells such as rounding or shrinking of the cells, granulation or vacuolization of the cytoplasm of the cells which shows that the nanoparticles are not toxic to the cells at these concentrations. However, for 100 μg/mL concentration the cell images show some signs of cell damage. Hence, our results are in agreement with that of MTT assay analysis for toxicity of the cells. The above data demonstrates that nanophosphors exhibit a negligible toxic effect on the cells at lower dosages and have the potential to be used for biomedical applications.

FTIR Analysis

FTIR spectra of uncapped and TEOA capped CaS:Eu nanophosphors were recorded in the range 4000–500 cm^{-1} and is shown in Fig. 10. The spectra consist of absorption bands at 2359 cm^{-1} and 1491 cm^{-1} corresponding to C-H stretching and bending vibrations [37, 38]. The FTIR spectrum of TEOA capped CaS: Eu nanoparticles (curve A) shows peaks at 3300 cm^{-1} which suggest the presence of O-H and N-H group. The peaks at 2900 cm^{-1} and at 1151 cm^{-1} are attributed to C-H and C-N stretching vibrations of TEOA [39]. The absorption peaks at 1218 cm^{-1}, 1066 cm^{-1} and 1010 cm^{-1} correspond to stretching of C-O bond present in TEOA [36–39]. The FTIR spectrum of uncapped CaS: Eu (curve B) also consists of peaks corresponding to O- H, C-H, and C-O bonding since it is prepared in 2- propanol. The broad peak ranging from 3600 to 3300 cm^{-1} in this case, arises due to O-H stretching vibration, and it can also be attributed to the formation of calcium hydroxide by absorption of moisture from the surroundings which is evident from XRD pattern portrayed in Fig. 3.Various absorption peaks and corresponding bonds in CaS: Eu nanophosphors are tabulated in Table 4. Thus, the presence of various bonds in the samples are confirmed by FTIR analysis.

Table 4 Various absorption peaks and corresponding bonds in CaS:Eu nanophosphors

Bond	Absorption peaks
O-H	3600 cm^{-1}, 3300 cm^{-1}, 3290 cm^{-1}
N-H	3300 cm^{-1}
C-N	1151 cm^{-1}
C-O	1218 cm^{-1}, 1211 cm^{-1}, 1066 cm^{-1},1010 cm^{-1}, 1000 cm^{-1}
C-H	2900 cm^{-1}, 2359 cm^{-1}, 1500 cm^{-1}

Conclusions

Highly fluorescent yellow emitting Eu^{3+} doped CaS nanophosphors were synthesized by a simple, cost-effective and eco-friendly wet chemical method. TEM and FESEM analysis confirmed the spherical morphology of the particles having a diameter within the nanoscale range. The emission color can be tuned from yellowish white to yellow by exciting the samples at wavelengths 335 nm and 395 nm. The PL emission spectra consist of highly intense peaks in the red region which confirms that Eu ions occupy non-centrosymmetric octahedral sites in the CaS nanocrystals. The optical bandgap of the TEOA capped CaS:Eu nanophosphors decreases with increase in the concentration of europium. The successful introduction of Eu^{3+} ions into the CaS host lattice is confirmed by XPS analysis. Cytotoxicity analysis of the nanoparticles on human cell lines using MTT assay revealed that the prepared nanoparticles are biocompatible over a wide range of concentrations which makes them a potential candidate for biomedical applications. FTIR analysis confirms the presence of various bonds in the prepared samples. The prepared nanoparticles had high PL intensity, purity and stability which makes them promising candidates for applications in solid-state lighting technology, optical displays, and bioimaging.

Acknowledgments Authors thank the Science and Engineering Research Board (SERB), Department of Science and Technology (DST), Government of India for financial support under the EMR scheme. Author S. Rekha thank University Grants Commission (UGC), Government of India for aid under FDP.

References

1. Lehman W, Ryan FM (1971) Cathodoluminescence of CaS : Ce^{3+} and CaS : Eu^{2+} phosphors. J Electrochem Soc 118:477–482
2. Crandall RS (1987) Mechanism of electroluminescence in alkaline earth sulfides. Appl Phys Lett 50:551–553
3. Kasano H, Megumi K, Yamamoto H (1987) Cathodoluminescence of $Ca_{1-x}MgS$: A (A=Eu or Ce). J Electrochem Soc 131:1953–1960
4. Yamamoto H, Megumi K Kasano H (1987) An orange-emitting phosphor (Ca, Mg)S.Mn for terminal display tubes. J Electrochem Soc 134:1571–1573
5. Marwaha GL, Singh N, Vij DR, Mathur VK (1980) Spectral variations and retrapping processes in CaS: Bi dosimeter. Radiat Eff 53: 25–31
6. Marwaha GL, Singh N, Nagpal JS, Mathur VK (1981) Operational importance of some physical parameters of TL phosphor CaS: Bi. Radiat Eff 55:85–90
7. Anuradha RI (2016) Europium doped nanophosphors and applications in in vitro optical bioimaging. J Integr Sci Technol 4(2):46–50
8. Sun BQ, Yi GS, Chen D, Zhou Y, Cheng J (2002) Synthesis and characterization of strongly fluorescent europium doped calcium sulfide nanoparticles. J Mater Chem 12:1194–1198
9. Haecke JE, Smet ZPF, Keyser KD, Poelman D (2007) Single crystal CaS: Eu and SrS: Eu luminescent particles obtained by solvothermal synthesis. J.Electrochem.Soc 154:J278–J282
10. Sawada N, Chen Y, Isobe T (2006) Low-temperature synthesis and photoluminescence of IIA-VIB nanophosphors doped with rare earth ions. J Alloys Compd 408:824–827
11. Burbano DC, Rodríguez EM, Dorenbos P, Capobianca JA (2014) The near –IR photostimulated luminescence of in CaS: Eu^{2+}/ Dy^{3+} nanophosphors. J Mater Chem C 2:228–233
12. Burbano DC, Sharma SK, Dorenbos P, Viana B, Capobianca JA (2015) Persistent and photostimulated red emission in CaS: Eu^{2+}, Dy^{3+} nanophosphors. Ad Opt Mater 3:551–557
13. Han M, Oh SJ, Park J, Park HL (1993) X-ray photoelectron spectroscopic studies of CaS: Eu and SrS: Eu phosphors. J Appl Phys 73(9):4546–4549
14. Rao CA, Rao NVP, Murthy KVR (2015) Synthesis, characterization and photoluminescence properties of CaS: Eu^{3+} and SrS: Eu^{3+} for white LED. APL 2(4):4–10. https://doi.org/10.1097/APL/62
15. Wu SH, Tseng CL, Lin FH (2010) A newly developed Fe-doped calcium sulfide nanoparticles with magnetic property for cancer hyperthermia. J Nanopart Res 12:1173–1185
16. Wu SH, Yang K, Tseng C, Chen J, Lin FH (2011) Silica modified Fe doped CaS nanoparticles for invitro and in vivo cancer hypothermia. J Nanopart Res 13:1139–1149
17. Forti K, Figueroa M, Torres B, Bernard F, Rivera D, Castro ME, Suarez E (2016) Calcium sulfide (CaS) nanostructure treatment on non-small cell lung cancer. FASEB J 30(1):1099.4
18. Kumar V, Kumar R, Lochab SP, Singh N (2006) Synthesis and characterization of bismuth doped calcium sulfide nanocrystallites. J Phys Condens Matter 18:5029–5036
19. Meerloo JV, Kaspers G, Cloos J (2011) Cell sensitivity assays: the MTT assay. In Cree IA (ed) Methods in molecular biology, cancer cell culture methods and protocols second edition. Humana Press, pp 237
20. Talarico LB, Zibetti RGM, Faria PCS, Scolaro LA, Duarte MER, Noseda MD, Pujol CA, Damonte EB (2004) Anti-herpes simplex virus activity of sulfated galactans from the red seaweeds Gymnogongrus griffithsiae and Cryptonemia crenulate. Int J Biol Macromol 34:63–41
21. Cullity BD (1978) Elements of X-ray diffraction, 2nd edn. Addison-Wiley Pub Co, Reading, Massachusetts, p 102
22. Luo W, Liu Y, Chen X (2015) Lanthanide doped semiconductor nanocrystals: electronic structures and optical properties. Sci China Mater 58:819–850
23. Huo Q, Tu W, Gio L (2017) Enhanced photoluminescence property and broad color emission of $ZnGa_2O_4$ phosphor due to the synergistic role of Eu and carbon dots. Opt Mater 72:305–312
24. Xu B, Li D, Huang Z, Tang C, Mo W, Ma Y (2018) Alleviating luminescence concentration quenching in lanthanide doped CaF_2 based nanoparticles through Na^+ ion doping. Dalton Trans 47: 7534–7540
25. Byun HJ, Kim J, Yang H (2009) Blue green and red emission from undoped and doped Zn Ga_2O_4 colloidal nanocrystals. Nanotechnology 20:495602
26. Wani JA, Dhoble NS, Kokode NS, Dhoble JS (2014) Synthesis and photoluminescence property of Re^{3+}activated Na_2Ca P_2O_7 phosphor. Adv Mater Lett 5(8):459–464
27. Blasse G (1986) Energy transfer between inequivalent Eu^{2+} ions. J Solid State Chem 62:207–211
28. Uitert LGV (1969) Characterization of energy transfer interactions between rare earth ions. J Electrochem Soc 114:1048–1053
29. Kubelka P, Munk F (1931) Ein Beitrag zur Optik der Farbanstriche. Zh Tekh Fiz 12:593–620
30. Kubelka P (1948) New contributions to the optics of intensely light-scattering materials. Part 1. J Opt Soc Am 38:448–457
31. Rekha S, Martinez A, Safeera TA, Anila EI (2017) Enhanced luminescence of Triethanolamine capped CaS nanophosphors synthesized by wet chemical method. J Lumin 190:94–99
32. Ahamed S, Zekry A (2010) A new and simple model for plasma and doping induced bandgap narrowing. J Electron Devices 8:293–299
33. Majid A, Ali A (2009) Band tailing effects in neon-implanted GaN. J Appl Phys 106:123528
34. Naumkin AV, Kraut-Vass A, Gaarenstroom SW, Powell CJ (2012) NIST x-ray photoelectron spectroscopy database, NIST Standard Reference Database 20, Version 4.1. https://doi.org/10.18434/T4T88K
35. Poornaprakash BP, Poojitha PT, Chalapathi U, Park SH (2016) Achieving room temperature ferromagnetism in ZnS nanoparticles via Eu^{3+} doping. Mater Lett 181:227–230
36. Kumar S, Prakash R, Choudhary RJ, Phase DM (2015) Structural, XPS and magnetic studies of pulsed laser deposited Eu_2O_3 thin film. Mater Res Bull 70:392–396
37. Coates J (2000) Interpretation of infrared spectra, a practical approach. In: Mayers RA (ed) Encyclopedia of analytical chemistry. John Wiley & Sons Ltd, Chichester, p 10815
38. Interpreting an infrared spectra: chemguide (2014). Available at http://www.chemguide.co.uk/analysis/ir/interpret. Accessed 17.05. 2018
39. Anandhan K, Thilak K (2015) Synthesis, FTIR, UV-vis and photoluminescence characterizations of triethanolamine passivated CdO nanostructures. Spectrochim Acta A Mol Biolmol Spectrosc 49:476–480